Reactions of CO and CO_2 with Gas-Phase Mo^+, MoO^+, and MoO_2^+

M. R. Sievers and P. B. Armentrout*

Department of Chemistry, University of Utah, Salt Lake City, Utah 84112

Received: September 14, 1998; In Final Form: October 26, 1998

Guided ion beam mass spectrometry is used to investigate the kinetic energy dependence of the bimolecular reactions of CO_2 and CO with Mo^+, MoO^+, and MoO_2^+. To obtain a more complete understanding of these systems, we probe MoO_2^+ and the intermediates, $Mo(CO_2)^+$, $OMo(CO)^+$, $OMo(CO_2)^+$, and $O_2Mo(CO)^+$, by collisional activation experiments with Xe. Thermochemical analyses of the reaction cross sections obtained in this study yield (in eV) $D_0(Mo^+-CO_2) = 0.51 \pm 0.07$, $D_0(OMo^+-CO_2) = 0.77 \pm 0.03$, $D_0(OMo^+-CO) = 0.80 \pm 0.08$, $D_0(O_2Mo^+-CO) = 0.92 \pm 0.17$, and $D_0(OMo^+-O) = 5.57 \pm 0.14$ eV. Additional features in some reaction cross sections are assigned to the formation of excited electronic states of the products, thereby allowing a speculative measurement of excitation energies for states of MoO^+ and MoO_2^+.

1. Introduction

The use of metal and metal oxide catalysts to convert carbon dioxide and carbon monoxide to more useful chemical materials is an active field of study.[1−10] One benefit of such chemistry is the removal of one abundant constituent of greenhouse gases, carbon dioxide. Concerning the metal of particular interest in this work, the oxides of molybdenum have been studied as hydrogenation catalysts of carbon dioxide and carbon monoxide.[11−16] Insight into the interaction of metal and metal oxides with CO or CO_2 can be garnered by examining analogous reactions in the gas phase using a guided ion beam mass spectrometer. Such work can elucidate the energetics of the reactions, their mechanisms, and details of the potential energy surfaces.

Previously, several groups have used ion cyclotron resonance (ICR) mass spectrometry to study the gas-phase interactions of CO_2 with metal cations and metal oxide cations at thermal energies.[17−23] We have used guided ion beam mass spectrometry to examine the reactions, $M^+ + CO_2 \rightarrow MO^+ + CO$ where M = V, Zr, ZrO, Nb, and NbO, and their reverse in detail over extended energy regimes.[24−26] These reactions exhibit cross sections with complicated energy dependencies. Analysis of these cross sections resulted in the determination of excitation energies for VO^+ and NbO^+, which were confirmed by photoelectron studies of VO and NbO.[27,28] Speculative excitation energies for ZrO^+, ZrO_2^+, and NbO_2^+, where no literature data are available, were also assigned. In addition, likely intermediates in these systems were independently produced and their thermochemistry determined. The present work extends this type of comprehensive study to molybdenum. Previous studies of gas-phase molybdenum oxide ions include studies of the reactions of MoO_x^+ ($x = 1-3$) with nitrous oxide, dihydrogen, small hydrocarbons, and aromatics.[29−32] Kretzschmar et al. also determined the energetics of the MoO_x^+ species and examined their electronic structures theoretically.[30]

One very important consideration in the systems studied here is the electronic states of the metal, metal monoxide, and metal dioxide cations. The ground state of Mo^+ is $^6S(4d^5)$, with excited states (in eV) at 1.46 (^6D, $5s^14d^4$), 1.88 (^4G, $4d^5$), 1.95 (^4P, $4d^5$), 2.08 (^4D, $4d^5$), and 2.78 (^2D, $4d^5$) above the ground state.[33] The ground states for the metal oxide and dioxide cation are unknown experimentally, but theoretical calculations have been performed. For the monoxide cation, early work by Broclawik[34,35] has been supplanted by higher levels calculations performed by Kretzschmar et al.[30] and Loock et al.[36] Both groups used density functional theory (DFT), including first-order relativistic corrections, while the former group included results (cited here) at the CASPT2D level including relativistic effects. Both studies find that MoO^+ has a $^4\Sigma^-$ ($1\sigma^22\sigma^21\pi^43\sigma^11\delta^2$) ground state with low-lying excited states of $^4\Pi$ ($1\sigma^22\sigma^21\pi^41\delta^22\pi^1$) and $^2\Delta$ ($1\sigma^22\sigma^21\pi^41\delta^3$). Kretzschmar et al. and Loock et al. find similar excitation energies of 0.59 and 0.77 eV, respectively, for the $^4\Pi$ state and 0.75 and 0.84 eV, respectively, for the $^2\Delta$ state. Other excited states include $^2\Sigma^+$ ($1\sigma^22\sigma^21\pi^41\delta^23\sigma^1$) calculated to lie 1.18 eV[36] above the ground state and $^6\Sigma^-$ ($1\sigma^22\sigma^21\pi^33\sigma^11\delta^2\,2\pi^1$) at 3.59 eV[30] above the ground state. For the molybdenum dioxide cation, Kretzschmar et al.[30] find a $^2A_1$ ground state with a low-lying $^2B_2$ state at 0.20 eV and a $^4A_2$ excited state at 2.40 eV. Overall, these considerations show that the reactions of ground-state $Mo^+(^6S)$ and $MoO^+(^4\Sigma^-) + CO_2(^1\Sigma_g^+)$ cannot form ground-state $MoO^+(^4\Sigma^-)$ and $MoO_2^+(^2A_1) + CO(^1\Sigma^+)$ products in spin-allowed processes.

The thermochemistry of the molybdenum oxide cations is also critical to understanding the processes observed in this work. Recent studies of the ion−molecule reactions of Mo^+ with various oxidants have established the Mo^+-O bond energy as 5.06 ± 0.02[37] and 5.12 ± 0.09 eV.[30] Here, we adopt the more precise value of $D_0(Mo^+-O) = 5.06 \pm 0.02$ eV. Less specific information is available for molybdenum dioxide cations. The JANAF tables[38] provide a heat of formation for neutral MoO_2 of -6 ± 13 kJ/mol, and this value is adopted in the compilation by Lias et al.[39] This corresponds to a bond energy for $OMo-O$ of 6.22 ± 0.26 eV. The IE of MoO_2 is listed by Lias et al.[39] as 9.2 eV with no uncertainty. DeMaria et al.[40] find $IE(MoO_2) = 9.4 \pm 0.6$ eV, while Choudary et al.[41] determine 9.8 ± 0.6 eV (although their value for IE(MoO) is quite high, 8.7 ± 0.6 eV, compared with the experimental value of 7.4504 eV[36]). In contrast to these "direct" electron impact ionization measurements, Kretzschmar et al.[30] use electron-transfer bracketing experiments to obtain $IE(MoO_2) = 8.7 \pm 0.3$ eV. Combined with their thermochemistry for MoO^+, this latter IE leads to a value for $D_0(OMo^+-O)$ of 5.29 ± 0.56 eV. Kretzschmar et al. also find that MoO^+ inefficiently reacts at thermal energies with CO_2 to form MoO_2^+ and argue that this

10.1021/jp983694v CCC: $15.00
Published on Web 12/08/1998

indicates $D_0(OMo^+-O) > D_0(OC-O) = 5.453 \pm 0.002$ eV.[39] Combining these results, they conclude that $D_0(OMo^+-O) = 5.68 \pm 0.22$ eV. For the purposes of examining the trends in the reactions studied here, we tentatively adopt this value but will refine it based on the results obtained here.

2. Experimental Section

2.1. General. These studies were performed using a guided ion beam tandem mass spectrometer. The instrument and experimental methods have been described previously.[42,43] Ions, formed as described below, were extracted from the source, accelerated, and focused into a magnetic sector momentum analyzer for mass analysis. The ions were decelerated to a desired kinetic energy and focused into an octopole ion guide that radially traps the ions. While in the octopole, the ions passed through a gas cell that contained the neutral reactant at pressures where multiple collisions were improbable (<0.30 mTorr). Single collision conditions were verified by examining the pressure dependence of the cross sections measured here. The product ions and the reactant ion beam drifted out of the gas cell, were focused into a quadrupole mass filter, and then detected by a secondary electron scintillation detector. Ion intensities were converted to absolute cross sections as described previously.[42] Uncertainties in the absolute cross sections are estimated at ±20%.

To determine the absolute zero and distribution of the ion kinetic energy, the octopole was used as a retarding energy analyzer.[42] The uncertainty in the absolute energy scale is ± 0.05 eV (laboratory). The full width at half-maximum (fwhm) of the ion energy distribution is 0.25−0.4 eV (laboratory). Lab energies were converted into center-of-mass energies using $E(\mathrm{CM}) = E(\mathrm{laboratory})m/(m + M)$ where M and m are the masses of the ion and neutral reactant, respectively. All energies stated in this paper are in the center-of-mass frame, unless noted otherwise.

2.2. Ion Source. The ion source used in this study was a dc discharge/flow tube (DC/FT) source described in previous work.[43] The DC/FT source utilized a molybdenum rod cathode held at 1.5−3 kV over which a flow of approximately 90% He and 10% Ar passed at a typical pressure of ~0.5 Torr. Ar^+ ions created in a direct current discharge were accelerated toward the molybdenum cathode, sputtering off atomic metal ions. The ions then underwent ~10^5 collisions with He and ~10^4 collisions with Ar in the meter long flow tube before entering the guided ion beam apparatus. To ensure that the Mo^+ ions were in their ground electronic state, methane gas was introduced ~25 cm downstream from the discharge at pressures of about 2 mTorr such that the ions are calculated to undergo 10^2-10^3 collisions with methane in the flow tube. Excited-state molybdenum cations have been shown to react efficiently at thermal energies with methane,[44] thus eliminating these states from the ion beam. This was verified by examining the reaction of methane quenched Mo^+ ions with methane in the collision cell and comparing that to results obtained when no methane was added in the flow tube. This work suggests that the Mo^+ ions produced in the DC/FT source were exclusively in their a^6S ground state.[45]

MoO^+ and MoO_2^+ were generated by allowing Mo^+ (created in the dc discharge) to react with O_2 introduced ~25 cm downstream into the flow tube at ~ 2 mTorr. $OMo^+(CO)$ and $O_2Mo^+(CO)$ were produced by allowing the Mo^+ to react with O_2 upstream in the flow tube and introducing CO downstream. $Mo^+(CO_2)$ and $OMo^+(CO_2)$ were produced by allowing the Mo^+ and MoO^+ to interact with CO_2 downstream in the flow tube. For all of these polyatomic ions, the large number of collisions between the ions and the bath gases should thermalize the ions both rotationally and vibrationally. We assume that these ions were in their ground electronic states and that the internal energy of these clusters was described by a Maxwell−Boltzmann distribution of rotational and vibrational states corresponding to 300 K. Previous work from this laboratory, including studies of N_4^+,[46] $Fe(CO)_x^+$ ($x = 1-5$),[47] $Cr(CO)_x^+$ ($x = 1-6$),[48] SiF_x^+ ($x = 1-4$),[49] and $H_3O^+(H_2O)_x$ ($x = 1-5$)[50] have shown that these assumptions are usually valid.

TABLE 1: Estimated Molecular Vibrational Frequencies

species		frequencies, (cm^{-1})[a]
CO_2[b]		667(2), 1333, 2349
CO[c]		2214.2
MoO^+[d]		894
MoO_2^+[e]		996, 966, 275
$Mo^+(CO_2)$		77, 144, 600, 935, 1176, 1745
$OMo^+(CO)$	(1)	35(2), 166, 221(2) + $\nu(MoO^+)$ + $\nu(CO)$
	(2)	20(2), 100, 150(2) + $\nu(MoO^+)$ + $\nu(CO)$
$OMo^+(CO_2)$	(1)	150(2), 200(2) + $\nu(MoO^+)$ + $\nu(CO_2)$
	(2)[f]	25, 77, 144, 200, 600, 935, 1067, 1176, 1745
$O_2Mo^+(CO)$	(1)	20(2), 100, 150(2) + $\nu(MoO_2^+)$ + $\nu(CO)$
	(2)	35(2), 166, 221(2) + $\nu(MoO_2^+)$ + $\nu(CO)$

[a] See text for details. Numbers in parentheses denote the degeneracy of the vibration. [b] Reference 54. [c] Reference 55. [d] Reference 56. [e] Reference 57. [f] $V^+(CO_2)$ frequencies from ref 24 and estimates for two bends (25 and 200 cm^{-1}).

2.3. Data Analysis. Previous theoretical[51,52] and experimental work[53] have shown that endothermic cross sections can be modeled using eq 1,

$$\sigma(E) = \sigma_0 \sum g_i (E + E_{\mathrm{rot}} + E_i - E_0)^n/E \qquad (1)$$

where σ_0 is an energy independent scaling parameter, E is the relative translational energy of the reactants, E_{rot} is the average rotational energy of the reactants, E_0 is the reaction threshold at 0 K, and n is an energy independent scaling parameter. The summation is over each vibrational state of the reactants having relative populations g_i and energies E_i.

The various sets of vibrational frequencies used in the data analysis are listed in Table 1. The frequencies for CO and CO_2 were taken from the literature.[54,55] The vibrational frequency for MoO^+ was taken to equal that of MoO, 893.5 cm^{-1}.[56] The frequencies for MoO_2^+ were estimated using frequencies taken from IR studies of MoO_2Cl_2.[57] The two higher frequencies used for MoO_2^+ were taken directly from the IR study, while the lower frequency is the average of the two low energy bending modes reported in the IR study. The vibrational frequencies for $Mo^+(CO_2)$ were estimated to equal the vibrational frequencies used previously for $V^+(CO_2)$.[24] The two low energy frequencies were adjusted for mass differences with a Morse potential scaling factor. The vibrational frequencies for $OMo^+(CO)$, $O_2Mo^+(CO)$, and $OMo^+(CO_2)$ were taken to equal the vibrational frequencies of MoO^+ or MoO_2^+, and CO or CO_2, plus several possible sets of frequencies for the OMo^+-CO or OMo^+-CO_2 modes that are similar to those we have used previously for $CrCO^+$ and $V^+(CO_2)$.[24,48] The frequencies used in this study were estimates and therefore were varied by ± 20%.

Before comparison with the data, the model of eq 1 is convoluted over the neutral and ion kinetic energy distributions using previously developed methods.[42] The parameters E_0, σ_0, and n are then optimized by using a nonlinear least-squares analysis in order to best reproduce the data. Reported values of E_0, σ_0, and n are mean values for each parameter from the best fits to several independent sets of data and uncertainties are one standard deviation from the mean. The listed uncertainties

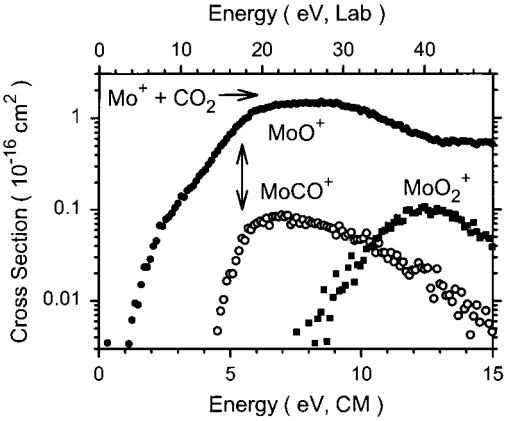

Figure 1. Product cross sections for $Mo^+ + CO_2$ as a function of collision energy in the center of mass frame (lower *x* axis) and laboratory frame (upper *x* axis). The arrow marks the bond dissociation energy of CO_2 at 5.45 eV.

TABLE 2: Bond Dissociation Energies at 0 K

bond	bond energy (eV)[a]
C−O	11.108 ± 0.005[b]
OC−O	5.453 ± 0.002[b]
Mo^+−O	5.06 ± 0.02[c]
OMo^+−O	5.68 ± 0.22,[d] 5.57 ± 0.14
Mo^+−CO	0.82 ± 0.13,[e] >0.46 ± 0.17
OMo^+−CO	0.80 ± 0.08
O_2Mo^+−CO	0.92 ± 0.17
Mo^+−CO_2	0.51 ± 0.07
OMo^+−CO_2	0.77 ± 0.03
Mo^+−Xe	>0.51 ± 0.07

[a] From this work, except as noted. [b] Reference 39. [c] Reference 37. [d] Reference 30. [e] Reference 58.

in E_0 values also include the uncertainty in the absolute energy scale and uncertainties introduced by the various vibrational frequencies with ±20% errors used for the complexes studied.

3. Results

3.1. $Mo^+ + CO_2$. Molybdenum cations react with carbon dioxide to form three products in reactions 2−4, as shown in Figure 1.

$$Mo^+ + CO_2 \rightarrow MoO^+ + CO \quad (2)$$

$$\rightarrow MoCO^+ + O \quad (3)$$

$$\rightarrow MoO_2^+ + C \quad (4)$$

Using literature thermochemistry in Table 2, reaction 2 is predicted to be endothermic by 0.39 ± 0.02 eV, while the MoO^+ cross section does not rise until an apparent threshold near 1 eV. At approximately 4 eV, the MoO^+ cross section changes slope and increases more rapidly. Near 6 eV, the MoO^+ cross section ceases to increase and remains relatively constant until ~9 eV. The change in cross section behavior near 6 eV can be attributed to the onset of dissociation of the MoO^+ product, reaction 5, which begins at D_0(OC−O) = 5.45 eV (Table 2).

$$Mo^+ + CO_2 \rightarrow Mo^+ + CO + O \quad (5)$$

Figure 2 shows the threshold region for reaction 2. To reproduce the data up to the region where the data begins to decline, two models were needed. The optimum parameters for these two models are given in Table 3. The first model has an E_0 value of 1.19 ± 0.15 eV, well above the thermodynamic

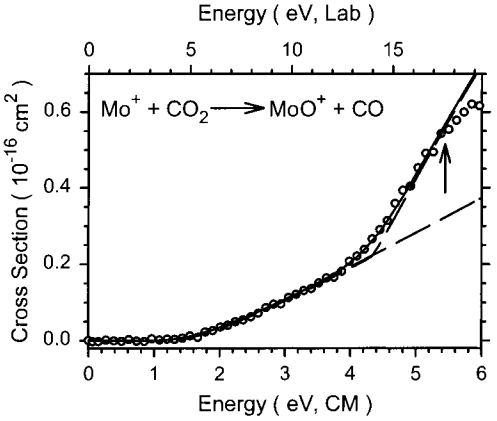

Figure 2. Product cross section for $Mo^+ + CO_2$ to form $MoO^+ + CO$ in the threshold region as a function of collision energy in the center of mass frame (lower *x* axis) and laboratory frame (upper *x* axis). The dashed lines show models with optimum parameters shown in Table 3. The solid line shows the sum of these two models convoluted with the experimental energy distributions.

threshold of 0.39 ± 0.02 eV. The second model has an E_0 value of 4.32 ± 0.06 eV. The individual models and their sum after convoluting over the experimental energy distributions are also shown in Figure 2.

The formation of $MoCO^+$ begins near 4.5 eV (Figure 1) and reaches a maximum near D_0(OC−O), indicating that its decline is due to reaction 5, dissociation of the $MoCO^+$ product. Analysis of this cross section with eq 1 yields an E_0 value for reaction 3 of 4.99 ± 0.17 eV (Table 3). This can be converted to a bond energy for Mo^+−CO of 0.46 ± 0.17 eV, which is somewhat lower than a theoretical value in the literature (Table 2).[58] This is probably because reaction 3 is suppressed by competition with the much more favorable reaction 2. Hence, we conservatively conclude that the Mo^+−CO bond energy measured here is a lower limit.

Formation of MoO_2^+ in reaction 4 is not observed until an apparent threshold near 8 eV. The thermodynamic threshold for this process calculated from literature thermochemistry (Table 2) is 5.82 ± 0.22 eV. Analysis of this cross section yields an E_0 value for MoO_2^+ formation (Table 3) of 7.8 ± 0.6 eV, considerably above this thermodynamic value. Either the literature thermochemistry is considerably in error, there is a substantial barrier to this reaction, or ground-state products are not formed. These possibilities are discussed below. The MoO_2^+ product cross section continues to rise until near 12 eV where it slowly begins to fall off. This decline is likely due to reactions 6 or 7,

$$Mo^+ + CO_2 \rightarrow MoO^+ + C + O \quad (6)$$

$$Mo^+ + CO_2 \rightarrow Mo^+ + O_2 + C \quad (7)$$

which have thermodynamic onsets at 11.50 ± 0.02 and 11.44 ± 0.01 eV, respectively. Given that MoO_2^+ dissociates exclusively to $MoO^+ + O$ (see section 3.9 below) upon collisional excitation with Xe, reaction 6 is probably the primary pathway.

3.2. $MoO^+ + CO$. The reaction of MoO^+ with CO forms two products through reactions 8−10 as shown in Figure 3.

$$MoO^+ + CO \rightarrow Mo^+ + O + CO \quad (8)$$

$$\rightarrow Mo^+ + CO_2 \quad (9)$$

$$\rightarrow MoO_2^+ + C \quad (10)$$

TABLE 3: Optimized Parameters of Equation 1 for the $MoCO_2^+$ System

reaction	σ_0	n	E_0, eV
(2) $Mo^+ + CO_2 \rightarrow MoO^+ + CO$	0.096 (0.033)	2.0 (0.3)	1.19 (0.15)
	1.14 (0.09)	1.2 (0.2)	4.32 (0.06)
(3) $\rightarrow MoCO^+ + O$	0.33 (0.11)	1.0 (0.3)	4.99 (0.17)
(4) $\rightarrow MoO_2^+ + C$	0.03 (0.03)	2.4 (0.7)	7.8 (0.6)
(10) $MoO^+ + CO \rightarrow MoO_2^+ + C$	0.68 (0.46)	1.5 (0.5)	7.1 (0.6)
(11) $Mo^+(CO_2) + Xe \rightarrow Mo^+ + CO_2 + Xe$	19.4 (3.1)	1.7 (0.3)	0.51 (0.07)
(13) $OMo^+(CO) + Xe \rightarrow MoO^+ + CO + Xe$			1.0 (0.5)

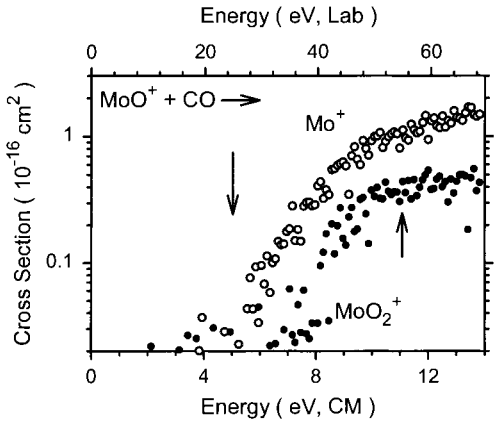

Figure 3. Product cross sections for $MoO^+ + CO$ as a function of collision energy in the center of mass frame (lower *x* axis) and laboratory frame (upper *x* axis). Arrows mark the bond dissociation energies of MoO^+ at 5.06 eV and CO at 11.11 eV.

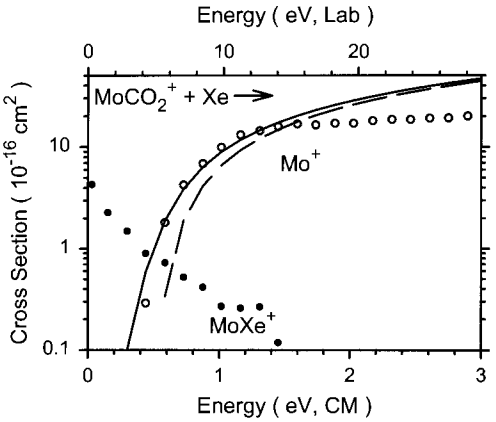

Figure 4. Product cross sections for $Mo^+(CO_2) + Xe$ as a function of collision energy in the center of mass frame (lower *x* axis) and laboratory frame (upper *x* axis). The dashed line is the model of eq 1 with the optimized parameters listed in Table 3 for the CID process. The solid line shows this model convoluted with the experimental energy distributions.

The cross section for Mo^+ rises slowly from an apparent threshold near 5 eV. This behavior is clearly associated with the simple collision-induced dissociation (CID) process, reaction 8, which has a thermodynamic threshold of 5.06 ± 0.02 eV (Table 2). However, direct comparison of this CID cross section to that obtained with Xe as the collision gas[37] shows that the CO cross section has a lower apparent threshold by about 1 eV. Either CO is a much more efficient collision gas or there are contributions from reaction 9 to the Mo^+ cross section. Indeed, careful examination of the Mo^+ cross section reveals very inefficient reactivity (<0.02 Å^2) below 5 eV. Previous work on the reactions of $MO^+ + CO$ [24−26] where M = V, Zr, and Nb have shown two obvious features in the M^+ product cross section that can clearly be related to the analogues of reactions 8 and 9. Generally, the thresholds observed for the lower energy reaction 9 analogues have corresponded to production of M^+ in electronically excited states that conserve spin in the overall process. In these cases, much more intense beams of the metal oxide cation reactant could be formed, such that the smaller cross section feature associated with reaction 9 could be observed readily. In the present case, literature thermochemistry predicts that the reaction to form $Mo^+(^6S) + CO_2(^1\Sigma^+_g)$ is 0.39 ± 0.02 eV exothermic. This reaction is clearly not occurring at its thermodynamic threshold, probably because it is a spin-forbidden process. The lowest energy pathway that conserves spin is formation of $Mo^+(a^4G) + CO_2$, which has a calculated thermodynamic threshold of 1.49 ± 0.02 eV. The inefficient reactivity can be reproduced using eq 1 with this energy as E_0. We conclude that CID dominates the production of Mo^+ in this system, but small contributions from reaction 9 with elevated onsets are indicated.

Starting about 7 eV, the MoO_2^+ cross section starts to rise. (A small nonzero cross section, <0.02 Å^2, observed below this energy is probably attributable to a trace contaminant in the CO reactant.) It continues to increase until near 10 eV where it levels off. The E_0 value obtained for this reaction, 7.1 ± 0.6 eV, exceeds the onset calculated from the literature thermochemistry in Table 2, 5.43 ± 0.22 eV. This result will be discussed further below.

3.3. $Mo^+(CO_2)$ + Xe. Collisional activation of $Mo^+(CO_2)$ with Xe yields two products formed in reactions 11 and 12 as shown in Figure 4.

$$Mo^+(CO_2) + Xe \rightarrow Mo^+ + CO_2 + Xe \qquad (11)$$

$$\rightarrow MoXe^+ + CO_2 \qquad (12)$$

The efficiency of reactions 11 and 12 combined with the failure to observe MoO^+ products is evidence that the CO_2 ligand is intact in the parent ion. The Mo^+ cross section rises rapidly from an apparent threshold less than 0.5 eV until about 1.5 eV where it remains relatively constant. Analysis of this cross section gives an E_0 value of 0.51 ± 0.07 eV (Table 3) which we assign as $D_0(Mo^+-CO_2)$. The ligand exchange product, $MoXe^+$, shows exothermic reaction behavior and can be reproduced using the Langevin−Gioumousis−Stevenson (LGS) model for ion-induced dipole reactions[59] after scaling by 0.02. From this observation, a lower limit to the Mo^+-Xe bond energy can be assigned, $D_0(Mo^+-Xe) > D_0(Mo^+-CO_2) = 0.51$ ± 0.07 eV. This lower limit seems reasonable considering that Cr^+, the first transition series congener of Mo^+, has a bond energy with Xe of 0.71 ± 0.10 eV.[48]

3.4. $OMo^+(CO)$ + Xe. When $OMo^+(CO)$ is activated by collisions with Xe, the only product observed is MoO^+, formed in reaction 13.

$$OMo^+(CO) + Xe \rightarrow MoO^+ + CO + Xe \qquad (13)$$

No Mo^+ or $MoXe^+$ products are observed, confirming that the reactant is no longer $Mo^+(CO_2)$ but a different isomer. Only a small beam intensity could be produced, hence this cross section is noisy and not displayed. The cross section rises slowly from

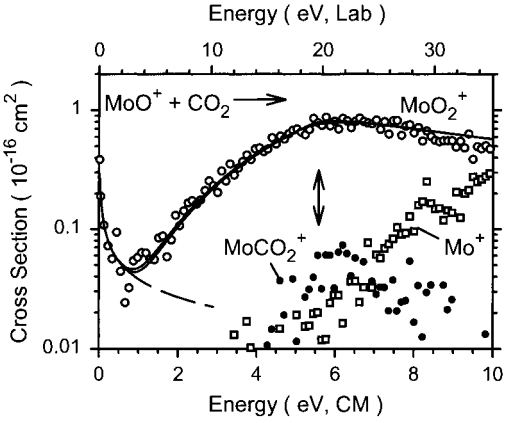

Figure 5. Product cross sections for $MoO^+ + CO_2$ as a function of collision energy in the center of mass frame (lower *x* axis) and laboratory frame (upper *x* axis). The lines show the exothermic model, the sum of that model with the endothermic model, and the sum convoluted with the experimental energy distributions. The arrow marks the bond energy of CO_2 at 5.45 eV.

an apparent threshold near 1 eV, but the large noise level prevents a meaningful analysis using eq 1. A rough analysis of the cross section for reaction 13 gives an E_0 value of 1.0 ± 0.5 eV, which we assign as $D_0(OMo^+-CO)$. Ligand exchange to form $OMo^+(Xe)$ might also occur but was not observed, perhaps because its magnitude is too small.

3.5. $MoO^+ + CO_2$. Three products are observed for the reaction of MoO^+ with CO_2, as shown in Figure 5. These are formed in reactions 14−16.

$$MoO^+ + CO_2 \rightarrow MoO_2^+ + CO \quad (14)$$

$$\rightarrow MoCO_2^+ + O \quad (15)$$

$$\rightarrow Mo^+ + CO_2 + O \quad (16)$$

The MoO_2^+ product cross section exhibits exothermic reaction behavior which has an $E^{-0.5}$ energy dependence, from 0 eV to near 1 eV. The low-energy exothermic feature for reaction 14 can be reproduced by scaling the LGS collision cross section by 10^{-3},[59] which indicates that MoO_2^+ is formed roughly once in every 1000 collisions. This result is in quantitative agreement with the observations of Kretzschmar et al. who found that this reaction had a reaction efficiency of 0.001 at thermal energies in an ion cyclotron resonance mass spectrometer.[30] Near 1 eV, the MoO_2^+ cross section starts to rise and continues rising until near 5.5 eV, consistent with the onset of reaction 17 at $D_0(OC-O) = 5.45$ eV.

$$MoO^+ + CO_2 \rightarrow MoO^+ + CO + O \quad (17)$$

The maximum in the MoO_2^+ cross section is also consistent with reaction 18 which has a thermodynamic onset of 5.39 ± 0.02 eV. This process seems unlikely given our failure to observe O_2 loss in the CID of $MoO_2^+ + Xe$ (see section 3.9 below).

$$MoO^+ + CO_2 \rightarrow Mo^+ + CO + O_2 \quad (18)$$

To reproduce the endothermic feature of the MoO_2^+ cross section, a model with $E_0 = 0.72 \pm 0.28$ eV was needed (Table 4). The sum of the exothermic and endothermic models reproduces the data nicely up to the point where the cross section begins to decline. To reproduce the data even further, a model that accounts for the dissociation of the product ion is included with eq 1.[60] This model includes a parameter *p*, which like *n* in eq 1 controls the energy dependence, and E_D, which defines the energy onset for dissociation.

The $MoCO_2^+$ cross section rises from an apparent threshold near 4−5 eV to about 6 eV and then falls off due to reaction 17. We determine an E_0 value for this process of 4.65 ± 0.08 eV (Table 4), which is consistent with calculated onsets for formation of OMo^+-CO, 4.45 ± 0.5 eV, and of Mo^+-CO_2, 4.55 ± 0.07 eV. It seems more reasonable that reaction 15 is analogous to reaction 3, such that the structure is OMo^+-CO. Then, the measured E_0 value can be converted to a OMo^+-CO bond energy of 0.80 ± 0.08 eV.

At higher energies, the simple collision-induced dissociation of MoO^+ to $Mo^+ + O$ by the collision gas CO_2 is observed, reaction 16. This cross section rises from an apparent threshold near 5.5 eV until about 11 eV where it plateaus. This cross section can be reproduced nicely with an E_0 value consistent with the BDE of MoO^+ reported previously (Table 2).[37]

3.6. $MoO_2^+ + CO$. The reaction of MoO_2^+ with CO results in the formation of two products, Figure 6, that can be formed in reactions 19−22.

$$MoO_2^+ + CO \rightarrow MoO^+ + CO_2 \quad (19)$$

$$\rightarrow MoO^+ + CO + O \quad (20)$$

$$\rightarrow Mo^+ + CO_2 + O \quad (21)$$

$$\rightarrow Mo^+ + CO + O_2 \quad (22)$$

The dominant product at all energies is the formation of MoO^+. This product can be formed in reaction 19, the reverse of reaction 14, and reaction 20, collision-induced dissociation. The cross section rises from an apparent threshold near 2 eV to about 5 eV, where the cross section rises more sharply until near 11 eV. To model this cross section over the entire energy region examined, two models are needed with optimum parameters given in Table 4. The thermodynamic threshold for reaction 19 is calculated to be 0.23 ± 0.22 eV, well below the onset determined by analysis with eq 1, 1.58 ± 0.18 eV (Table 4). The E_0 value of 5.52 ± 0.16 eV (Table 4) obtained from the high energy feature of this cross section clearly corresponds to simple CID, reaction 20, and agrees with the literature thermodynamic threshold of 5.68 ± 0.22 eV = $D_0(OMo^+-O)$.

Formation of Mo^+ is observed at high energies and could result from reactions 21 and 22. The cross section rises from an apparent threshold near 6 eV until about 8 eV where it plateaus. The competition of this channel with the thermodynamically favored MoO^+ channel accounts for its small cross section. The E_0 value obtained for this channel, 5.32 ± 0.34 eV (Table 4), is consistent with calculated thermodynamic thresholds of 5.29 ± 0.22 and 5.63 ± 0.22 eV for reactions 21 and 22, respectively. Reaction 21 is more plausible as O_2 loss is not observed when MoO_2^+ is collisionally activated by Xe (see section 3.9 below).

3.7. $OMo^+(CO_2) + Xe$. The collision-induced dissociation of the $OMo^+(CO_2)$ complex cation with Xe results in one product being formed in reaction 23.

$$OMo^+(CO_2) + Xe \rightarrow MoO^+ + CO_2 + Xe \quad (23)$$

The quality of the data is comparable to that shown for MoO_2^+

TABLE 4: Optimized Parameters of Eq 1 for the $MoCO_2^+$ System

reaction	σ_0	n	E_0, eV
(14) $MoO^+ + CO_2 \rightarrow MoO_2^+ + CO^a$	0.089 (0.053)	2.6 (0.3)	0.72 (0.28)
(15) $\rightarrow MoCO_2^+ + O$	0.22 (0.01)	1.5 (0.2)	4.65 (0.08)
(16) $\rightarrow Mo^+ + O + CO_2$	0.062 (0.036)	2.7 (0.3)	5.02 (0.37)
(19) $MoO_2^+ + CO \rightarrow MoO^+ + CO_2$	0.028(0.010)	2.0 (0.2)	1.58 (0.18)
(20) $\rightarrow MoO^+ + O + CO$	1.57 (0.37)	1.5 (0.1)	5.52 (0.16)
(21) $\rightarrow Mo^+ + CO_2 + O$	0.087 (0.026)	1.2 (0.2)	5.32 (0.34)
(23) $OMo^+(CO_2) + Xe \rightarrow MoO^+ + CO_2 + Xe$	45.7 (0.9)	1.4 (0.2)	0.77 (0.03)
(24) $O_2Mo^+(CO) + Xe \rightarrow MoO_2^+ + CO + Xe$	7.5 (3.6)	3.3 (0.7)	0.92 (0.17)
(25) $MoO_2^+ + Xe \rightarrow MoO^+ + O + Xe$	0.25 (0.15)	2.1 (0.3)	5.33 (0.43)

[a] Parameters for the high-energy part of the modeling (see text) were $p = 2$ and $E_D = 5.43 \pm 0.07$ eV.

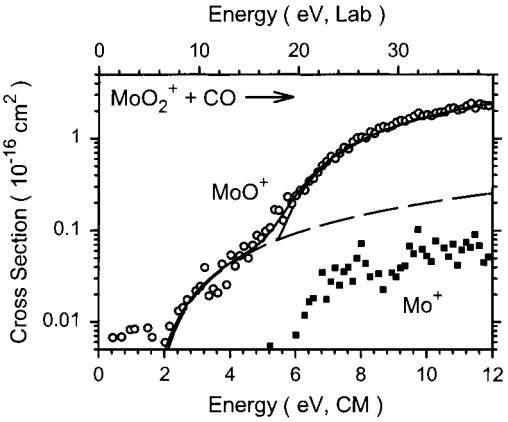

Figure 6. Product cross sections for $MoO_2^+ + CO$ as a function of collision energy in the center of mass frame (lower *x* axis) and laboratory frame (upper *x* axis). The dashed line is the model of eq 1 with the optimized parameters listed in Table 4 for the formation of $MoO^+ + CO_2$. Above 5 eV, a second dashed line shows the sum of this model with one for CID using the optimized parameters listed in Table 4. The solid line shows the sum of these two models convoluted with the experimental energy distributions.

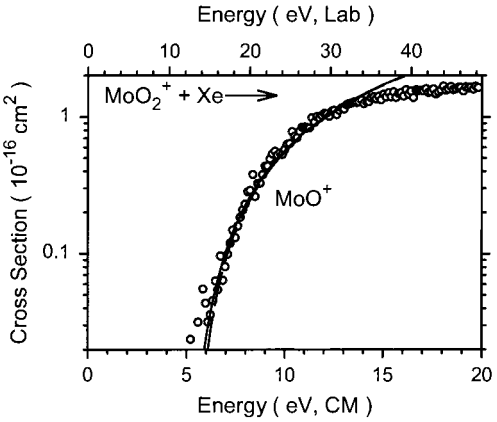

Figure 7. Product cross sections for $MoO_2^+ + Xe$ as a function of collision energy in the center of mass frame (lower *x* axis) and laboratory frame (upper *x* axis). The dashed line is the model of eq 1 with the optimized parameters listed in Table 4 for the CID process. The solid line shows this model convoluted with the experimental energy distributions.

(section 3.9). This cross section rises from an apparent threshold near 0.4 eV and then continues increasing until near 1.5 eV at which point it levels off with a magnitude of about 25 Å^2. The fact that loss of CO_2 is the lowest energy pathway for this complex to dissociate indicates that the structure for this molecule is MoO^+ ligated by CO_2 and not some other isomer of $MoCO_3^+$. From the analysis of this process, we get an E_0 value of 0.77 ± 0.03 eV (Table 4) which we assign to $D_0(OMo^+-CO_2)$. Ligand exchange to form $OMo^+(Xe)$ might also occur but was not observed, perhaps because its magnitude is too small.

3.8. $O_2Mo^+(CO) + Xe$. Collision-induced dissociation of the $O_2Mo^+(CO)$ complex yields one product in reaction 24.

$$O_2Mo^+(CO) + Xe \rightarrow MoO_2^+ + CO + Xe \qquad (24)$$

This observation ensures that the identity of the complex is MoO_2^+ ligated by CO. Failure to observe competitive O_2 loss also suggests a covalently bound molybdenum dioxide cation. The quality of the data is comparable to that shown for MoO_2^+ (section 3.9). This cross section rises rapidly from an apparent threshold near 0.8 eV and levels off near 3 eV with a magnitude of about 12 Å^2. Analysis of this cross section gives an E_0 value of 0.92 ± 0.17 eV (Table 4) which we assign to $D_0(O_2Mo^+-CO)$. Ligand exchange to form $O_2Mo^+(Xe)$ might also occur but was not observed, perhaps because its magnitude is too small.

3.9. $MoO_2^+ + Xe$. Collision-induced dissociation of MoO_2^+ with Xe gives only one product in reaction 25 as shown in Figure 7.

$$MoO_2^+ + Xe \rightarrow MoO^+ + O + Xe \qquad (25)$$

The MoO^+ cross section rises rapidly from an apparent threshold of 5−6 eV. Analysis of the energy dependence of this cross section results in $D_0(OMo^+-O) = 5.33 \pm 0.43$ eV (Table 4). It is possible that this value is an upper limit because previous work done on the CID of diatomic metal oxide cations with Xe has shown the E_0 values measured can be higher than bond energies determined using results from other reactions (e.g., $M^+ + CO$ or $O_2 \rightarrow MO^+ + C$ or O).[37]

4. Discussion

4.1. MoO_2^+ Thermochemistry. Our analyses of the cross sections for reactions 4, 10, 14, 19, 20, 21, and 25 provide E_0 values that can be converted to OMo^+-O bond dissociation energies (BDEs) of 3.7 ± 0.6, 4.0 ± 0.6, > 5.45, 7.03 ± 0.18, 5.52 ± 0.16, 5.71 ± 0.34, and 5.33 ± 0.43 eV, respectively. Except for the values derived from reactions 4, 10, and 19, the BDEs are consistent with each other and with the literature value of 5.68 ± 0.22 eV.[30] Reactions 4 and 10 may suffer from severe competition with favored reaction pathways having lower endothermicities or possibly from barriers along the potential energy surface. However, we think it most likely that the thresholds for reactions 4 and 19 may correlate with the formation of products in electronically excited states, as discussed further in the following section. The average OMo^+-O BDE obtained from the remaining reactions, 20, 21, and 25, is 5.52 ± 0.19 eV, and this also agrees well with the most precise

value obtained from reaction 20. A lower limit to this bond energy is also established by the observation of reaction 14, both in our work (Figure 5) and that of Kretzschmar et al.[30] Thus, our best value for $D_0(OMo^+-O)$ is 5.57 ± 0.14 eV. This agrees nicely with the experimental limits recommended by Kretzschmar et al.,[30] 5.68 ± 0.22 eV, and with a theoretical value of 5.51 eV determined in the same work. Combined with literature information outlined in the Introduction, our bond energy corresponds to $IE(MoO_2) = 8.44 \pm 0.37$ eV. This is consistent with the electron transfer (ET) reactions studied by Kretzschmar et al. in which no ET was observed with benzene (IE = 9.25 eV), rapid ET was observed with cycloheptatriene (IE = 8.29 eV), and slow ET was observed with toluene (8.82 eV).[30] From these observations, they assigned $IE(MO_2)$ as 8.7 ± 0.3 eV, in agreement with the value derived here.

4.2. Excitation Energies for MoO^+ and MoO_2^+. In our previous studies of the interaction of metal cations with CO_2,[24-26] multiple features for the reaction cross sections were assigned to the formation of the metal oxide cation in different excited electronic configurations. The appearance of multiple features was attributed to varying reaction efficiencies depending on whether the reaction conserves spin. Modeling the kinetic energy dependence of these features allowed speculative electronic excitation energies to be determined for those states. In the vanadium and niobium studies, substantial prior work had been done in determining the electronic spectrum of the metal oxide cation.[27,28] In these cases, the excitation energies that we determined could be assigned to particular states with a great deal of certainty. To our knowledge, there has been no experimental and little theoretical work (outlined in the Introduction) done on the MoO^+ excited states. Among the reactions studied here, processes 2, 4, and 19 are all candidates for determining excitation energies as these reactions are spin-forbidden to form ground-state products. Comparison of the measured E_0 values for these processes to the thermodynamic thresholds can be used to ascertain speculative excitation energies for the metal oxide products, assuming that there exist no barriers in excess of the endothermicity of these processes.

In the case of reaction 2, ground-state reactants are $Mo^+(a^6S) + CO_2(^1\Sigma_g^+)$ such that formation of the $MoO^+ + CO(^1\Sigma^+)$ products should be enhanced if the MoO^+ species has a sextet spin state. Hence, we attribute the high energy feature observed in this cross section (Figure 2) starting near 4 eV to formation of a sextet state of MoO^+. The E_0 value measured for this process (Table 3) lies 3.93 ± 0.06 eV above the calculated thermodynamic value. This energy is assigned to the lowest energy sextet state of MoO^+, which can be formed from the $^4\Sigma^-(1\sigma^2 2\sigma^2\ 1\pi^4 3\sigma^1 1\delta^2)$ ground state by promoting a bonding 1π electron into a 2π antibonding orbital resulting in a $^6\Delta/^6\Sigma^-$ $(1\sigma^2 2\sigma^2 1\pi^3 3\sigma^1 1\delta^2 2\pi^1)$ state. Our value for this excitation energy is comparable to that calculated for a $^6\Sigma^-$ state by Kretzschmar et al.,[30] 3.59 eV.

In the case of reaction 4, the reaction should evolve along a sextet surface correlating with the $Mo^+(a^6S) + CO_2(^1\Sigma_g^+)$ ground-state reactants. The neutral carbon atom product has a ^3P ground state such that spin can be conserved if the MoO_2^+ product is formed in a quartet state, but not the $^2A_1$ ground state. The E_0 value measured for this process, 7.8 ± 0.6 eV, lies 1.9 ± 0.6 eV above the calculated thermodynamic threshold of 5.93 ± 0.14 eV. This speculative excitation energy is within experimental error of the 2.41 eV value calculated for the $^4A_2$ state of MoO_2^+ by Kretzschmar et al.[30]

In the case of reaction 19, the $MoO_2^+(^2A_1) + CO\ (^1\Sigma^+)$ ground-state reactants will preferentially form $CO_2\ (^1\Sigma_g^+)$ along with MoO^+ in an excited doublet state. As the E_0 value we determine for MoO^+ (Table 4) lies 1.46 ± 0.23 eV above the thermodynamic threshold for this process, it is feasible that this measured threshold corresponds to formation of products along a spin-allowed pathway. This value does not correspond to calculated excitation energies for the lowest doublet state of MoO^+, the $^2\Delta$, of 0.75[30] and 0.84[36] eV, but is similar to that for MoO^+ $(^2\Sigma^+)$ of 1.18 eV.[30] The spin-forbidden pathway leading to ground-state MoO^+ $(^4\Sigma^-)$ is presumably too inefficient to observe.

The oxygen atom transfer reactions of Mo^+ and MoO^+ with CO_2, processes 2 and 14, are both observed to have E_0 values in excess of the values calculated for production of ground-state product by similar amounts, 0.80 ± 0.15 and 0.84 ± 0.31 eV, respectively. It is possible that these features are associated with the production of excited states of MoO^+ and MoO_2^+; in which case, the small magnitudes of these cross section features suggest that they correspond to spin-forbidden pathways. For the MoO^+ product, these could be either the $^4\Pi$ which has been calculated to lie 0.59[30] and 0.77[36] eV above the $^4\Sigma^-$ ground state or the $^2\Delta$ state calculated to 0.75[30] and 0.84[36] eV above the ground state. For the MoO_2^+ product, however, no states with excitation energies similar to 0.84 have been calculated. Another possible explanation for these elevated thresholds relies on the observation that dissociation of $CO_2\ (^1\Sigma_g^+)$ to $CO\ (^1\Sigma^+) + O(^3P)$ ground-state species is spin-forbidden while the spin-allowed dissociation asymptote, $CO\ (^1\Sigma^+) + O(^1D)$, lies 1.97 eV higher in energy. Hence there is a barrier in excess of the OC−O bond dissociation energy of 5.453 eV that must be overcome to remove O from CO_2 in a spin-allowed process. To form ground-state products, MoO^+ $(^4\Sigma^-)$ and MoO_2^+ $(^2A_1)$, respectively, the Mo^+ (^6S) and MoO^+ $(^4\Sigma^-)$ reactants must couple with O (^3P) such that reactions 2 and 14 must involve interaction of the cationic reactants with both the singlet and triplet surfaces of CO_2. Thus, it seems plausible that the 0.8 eV barriers observed for these reactions are both reflections of the complex potential energy surface associated with oxygen atom abstraction from CO_2. This possibility is illustrated in more detail in the next section.

4.3. $MoCO_2^+$ Potential Energy Surface. To understand these experiments in detail, we take the point of view that the experiments performed in this study ($Mo^+ + CO_2$, $MoO^+ + CO$, and CID of Mo^+-CO_2 and OMo^+-CO) probe four separate places on the same set of potential energy surfaces for the $MoCO_2^+$ system. The electronic states for the $Mo^+ + CO_2$ and $MoO^+ + CO$ asymptotes, described in the Introduction and further in the discussion, are shown in Figure 8. The measurement of $D_0(Mo^+-CO_2)$ and $D_0(OMo^+-CO)$ determine the well depths of these intermediates for ground-state species. We anticipate the bonding of Mo^+ with CO_2 and MoO^+ with CO is dominated by donation of ligand electrons into an empty 5s orbital on the metal and weak back-donation of electron density from metal $4d\pi$ orbitals into empty π-symmetry orbitals of the ligand. Bonding is enhanced when the 5s orbital is empty and the $4d\pi$ orbitals are occupied. Using this argument, we anticipate that Mo^+ states where the 5s orbital is occupied will have smaller bond energies. For Mo^+, the $a^4G\ (4d^5)$ state binds more strongly to CO_2 than the $a^6S\ (4d^5)$ state because two electrons, instead of one, can be used for π-back-bonding[61] into a single orbital on the ligand. For simplicity, we show in Figure 8 only the lowest energy Mo^+ states of each spin.

The asymptotes of $Mo^+ + CO_2$ and $MoO^+ + CO$ must now be connected. The excited-state $Mo^+(a^4G) + CO_2$ reactants evolve to ground-state $OMo^+(CO)$ and on to $MoO^+(^4\Sigma^-) +$

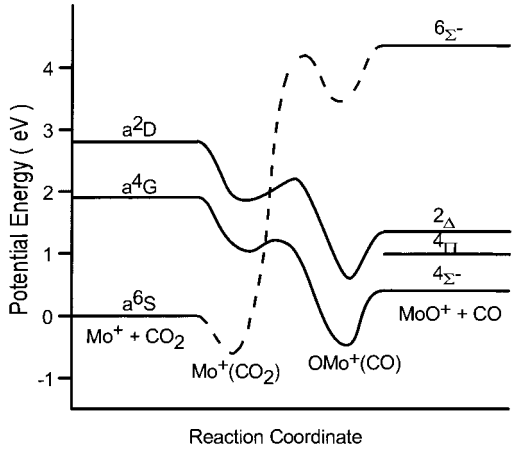

Figure 8. The potential energy surfaces for the interaction of Mo^+ with CO_2 deduced in the present study. Solid lines show quartet and doublet surfaces while dashed lines indicate sextet surfaces. Energies of the asymptotes and the $Mo^+(CO_2)$ and $OMo^+(CO)$ ground states are shown quantitatively. All other features are estimated. See text.

$CO(^1\Sigma^+)$ ground-state products. $Mo^+(a^2D) + CO_2(^1\Sigma_g^+)$ and $Mo^+(a^6S) + CO_2(^1\Sigma_g^+)$ reactants diabatically correlate to $MoO^+(^2\Delta) + CO(^1\Sigma^+)$ and $MoO^+(^6\Sigma^-) + CO(^1\Sigma^+)$ product asymptotes, respectively. Energies of the barriers between the $Mo^+(CO_2)$ and $OMo^+(CO)$ species on each surface are unknown as are the energies of the crossing points among the surfaces having different spins.

With these qualitative potential energy surfaces, we can now understand most of our experimental observations. $Mo^+(a^6S)$ reacts with CO_2 to form $MoO^+(^4\Sigma^-) + CO(^1\Sigma^+)$ in an endothermic reaction. The E_0 value determined for this reaction lies higher than the asymptotic energy of the products by 0.80 $\pm$ 0.15 eV. This is plausibly assigned as the barrier separating the $Mo^+(CO_2)$ and $OMo^+(CO)$ intermediates, the energy of the crossing between the sextet and quartet surfaces, or possibly as the production of the excited $^4\Pi$ or $^2\Delta$ state of MoO^+ (although why either state would be formed preferentially over the $^4\Sigma^-$ ground state is unclear). As the kinetic energy is increased, $Mo^+(a^6S)$ reacts more efficiently along a spin-conserved pathway to form $MoO^+(^6\Sigma^-) + CO$ beginning 3.93 $\pm$ 0.06 eV above ground-state products. When $MoO^+(^4\Sigma^-)$ reacts with $CO(^1\Sigma^+)$, the dominant reaction is simple collision-induced dissociation, although very inefficient production of $Mo^+ + CO_2$ is observed. Although this reaction is exothermic, a barrier to this process is observed. It seems likely that this reverse reaction will have a similar propensity for conserving spin as does the $Mo^+ + CO_2$ reaction, such that excited quartet states of Mo^+ should be the primary products in this reaction, consistent with the elevated E_0 value for this reaction. When $Mo^+(CO_2)$ and $OMo^+(CO)$ are collisionally activated, simple CID of the CO ligand dominates the product spectra. This is clearly because ligand loss is much more facile and energetically favorable than the rearrangements necessary to form alternative products. In addition, the potential energy surfaces in Figure 8 show that rearrangement processes do not conserve spin if ground-state products are formed, making these channels improbable. If spin is conserved, formation of these products is even more endothermic, lowering their probability even further.

The potential energy surfaces associated with the $MoCO_3^+$ system should exhibit many similarities to that shown for the $MoCO_2^+$ system. We decline to show such a potential energy surface given the uncertainties in the asymptotes for states of both the MoO^+ reactants and MoO_2^+ products.

Acknowledgment. This research is supported by the National Science Foundation, Grant 9530412.

References and Notes

(1) Avila, Y.; Barrault, J.; Pronier, S.; Kappenstein, C. *Appl. Catal. A.* **1995**, *132*, 97.
(2) Miciukiewicz, J.; Mang, T. *Appl. Catal. A.* **1995**, *122*, 151.
(3) Fujita, T.; Nishiyama, Y.; Ohtsuka, Y.; Asami, K.; Kusakabe, K.-I. *Appl. Catal. A.* **1995**, *126*, 245.
(4) Weimer, T.; Schaber, K.; Specht, M.; Bandi, A. *Energy Convers. Manage.* **1996**, *37*, 1351.
(5) Yanagisawa, Y. *Energy Convers. Manage.* **1995**, *36*, 443.
(6) Park, S.-E.; Nam, S. S.; Choi, M. J.; Lee, K. W. *Energy Convers. Manage.* **1995**, *36*, 573.
(7) Saito, M.; Fujitani, T.; Takahara, I.; Watanabe, T.; Takeuchi, M.; Kanai, Y.; Moriya, K.; Kakumoto, T. *Energy Convers. Manage.* **1995**, *36*, 577.
(8) Hirano, M.; Akano, T.; Imai, T.; Kuroda, K. *Energy Convers. Manage.* **1995**, *36*, 585.
(9) Otorbaev, D. K. *Chem. Phys.* **1995**, *196*, 543.
(10) Sahibzada, M.; Chadwick, D.; Metcalfe, I. S. *Catal. Today* **1996**, *29*, 367.
(11) Bandi, A. *J. Electrochem. Soc.* **1990**, *137*, 2157.
(12) Tatsumi, T.; Muramatsu, A.; Tominaga, H. *Proc. Annu. Int. Pittsburgh Coal Conf.* **1990**, *7*, 612.
(13) Tatsumi, T.; Muramatsu, A.; Yokota, K.; Tominaga, H. *Stud. Surf. Sci. Catal. 36 (Methane Convers.)* **1988**, *36*, 219.
(14) Kuznetsova, L. I.; Karelin, D. A.; Chumakov, V. G.; Kachin, S. V. *React. Kinet. Catal. Lett.* **1991**, *44*, 401.
(15) Jouchang, X.; Naasz, B. M.; Somorjai, G. A. *Appl. Catal.* **1986**, *27*, 233.
(16) Tatsumi, T.; Muramatsu, A.; Tominaga, H. *J. Catal.* **1986**, *101*, 533.
(17) Kappes, M. M.; Staley, R. H. *J. Phys. Chem.* **1981**, *85*, 942.
(18) Kappes, M. M.; Staley, R. H. *J. Am. Chem. Soc.* **1981**, *103*, 1286.
(19) Kikthenko, A. V.; Goncharov, V. B.; Zamaraev, K. I. *Catal. Lett.* **1993**, *21*, 353.
(20) Izod, T. P. J.; Kistiakowsky, G. B.; Matsuda, S. *J. Chem. Phys.* **1972**, *76*, 2833.
(21) Matsuda, S. *J. Chem. Phys.* **1972**, *57*, 807.
(22) Matsuda, S. *J. Phys. Chem.* **1972**, *76*, 2833.
(23) Wesendrup, R.; Schwarz, H. *Angew. Chem., Int. Ed. Engl.* **1995**, *34*, 2033.
(24) Sievers, M. R.; Armentrout, P. B. *J. Chem. Phys.* **1995**, *102*, 754.
(25) Sievers, M. R.; Armentrout, P. B. *Int. J. Mass Spectrom.* **1998**. Accepted for publication.
(26) Sievers, M. R.; Armentrout, P. B. *Int. J. Mass Spectrom.* **1998**. Accepted for publication.
(27) Dyke, J. M.; Gravenor, B. W. J.; Hastings, M. P.; Morris, A. *J. Phys. Chem.* **1985**, *89*, 4613.
(28) Dyke, J. M.; Ellis, A. M.; Fehér, M.; Morris, A.; Paul, A. J.; Stevens, J. C. H. *J. Chem. Soc., Faraday. Trans. 2* **1987**, *83*, 1555.
(29) Cassady, C. J.; McElvany, S. W. *Organometallics* **1992**, *11*, 2367.
(30) Kretzschmar, I.; Fiedler, A.; Harvey, J. N.; Schröder, D.; Schwarz, H. *J. Phys. Chem. A* **1997**, *101*, 6252.
(31) Kretzschmar, I.; Schröder, D.; Schwarz, H. *Int. J. Mass Spectrom. Ion Processes* **1997**, *167/168*, 103.
(32) Fialko, E. F.; Kikhtenko, A. V.; Goncharov, V. B.; Zamaraev, K. I. *J. Phys. Chem. A* **1997**, *101*, 8607.
(33) Moore, C. E. Atomic energy levels (U.S. Government Printing Office: Circular No. 467; Washington, DC, 1952.
(34) Broclawik, E. *Catal. Today* **1995**, *23*, 379.
(35) Broclawik, E. *Int. J. Quantum Chem.* **1995**, *56*, 779.
(36) Loock, H.-P.; Simard, B.; Wallin, S.; Linton, C. Unpublished work.
(37) Sievers, M. R.; Chen, Y.-M.; Armentrout, P. B. *J. Chem. Phys.* **1996**, *105*, 6322.
(38) Chase, M. W., Jr.; Davies, C. A.; Downey, J. R., Jr.; Frurip, D. J.; McDonald, R. A.; Syverud, A. N. *J. Phys. Chem. Ref. Data Suppl.* **1985**, *14*, 1.
(39) Lias, S. G.; Bartmess, J. E.; Liebman, J. F., J. L.; Levin, R. D.; Mallard, W. G. *J. Phys. Chem. Ref. Data, Suppl.* **1988**, *17*, Suppl. 1.
(40) DeMaria, G.; Burns, R. P.; Drowart, J.; Inghram, M. G. *J. Chem. Phys.* **1960**, *32*, 1373.
(41) Choudary, U. V.; Gingerich, K. A.; Kingcade, J. E. *J. Less-Common Met.* **1975**, *42*, 111.
(42) Ervin, K. M.; Armentrout, P. B. *J. Chem. Phys.* **1985**, *83*, 166.
(43) Schultz, R. H.; Armentrout, P. B. *Int. J. Mass Spectrom. Ion. Processes* **1991**, *107*, 29.
(44) Sievers, M. R.; Armentrout, P. B. Work in progress.
(45) Sievers, M. R.; Chen, Y.-M.; Elkind, J. L.; Armentrout, P. B. *J. Phys. Chem.* **1996**, *100*, 54.
(46) Schultz, R. H.; Armentrout, P. B. *J. Chem. Phys.* **1992**, *96*, 1046.

(47) Schultz, R. H.; Crellin, K. C.; Armentrout, P. B. *J. Am. Chem. Soc.* **1992**, *113*, 8590.

(48) Khan, F. A.; Clemmer, D. E.; Schultz, R. H.; Armentrout, P. B. *J. Phys. Chem.* **1993**, *97*, 7978.

(49) Fisher, E. R.; Kickel, B. L.; Armentrout, P. B. *J. Phys. Chem.* **1993**, *97*, 10204.

(50) Dalleska, N. F.; Honma, K.; Armentrout, P. B. *J. Am. Chem. Soc*. **1993**, *115*, 12125.

(51) Aristov, N.; Armentrout, P. B. *J. Am. Chem. Soc.* **1986**, *108*, 1806 and references therein.

(52) Chesnavich, W. J.; Bowers, M. T. *J. Phys. Chem.* **1979**, *83*, 900.

(53) Armentrout, P. B. In *Advances in Gas-Phase Ion Chemistry*; Adams, N. G., Babcock, L. M., Eds.; JAI: Greenwich, 1992; Vol. 1, pp 83−119.

(54) Shimanouchi, T. *Table of Molecular Vibrational Frequencies, Consolidated*; National Bureau of Standards, Vol. I.; U.S. Department of Commerce: Washington, DC, 1972; Vol. I.

(55) Huber, K. P.; Herzberg, G. *Molecular Spectra and Molecular Structure IV. Constants of Diatomic Molecules*; Van Nostrand Reinhold Company: New York, 1979; Vol. IV.

(56) Bates, J. K.; Gruen, D. M. *J. Mol. Spectrosc*. **1979**, *78*, 284.

(57) Neikirk, D. L.; Fagerli, J. C.; Smith, M. L.; Mosman, D.; Devore, T. C. *J. Mol. Struct*. **1991**, *244*, 165.

(58) Barnes, L. A.; Rosi, M.; Bauschlicher, C. W., Jr. *J. Chem. Phys.* **1990**, *93*, 609.

(59) Gioumousis, G.; Stevenson, D. P. *J. Chem. Phys*. **1958**, *29*, 294.

(60) Weber, M. E.; Elkind, J. L.; Armentrout, P. B., *J. Chem. Phys.* **1986**, *84*, 1521.

(61) Dedieu, A.; Bo, C.; Ingold, F. In *Metal−Ligand Interactions: From Atoms, to Clusters, to Surfaces;* Salahub, D. R., Russo, N., Eds.; NATO Advanced Study Institute, Series C; Kluwer: Dordrecht, 1992; Vol. 378, p 175.